FULL PAPER

Magnetic Resonance in Medicine 00:00–00 (2017)

Real-Time Monitoring of Tissue Displacement and Temperature Changes during MR-Guided High Intensity Focused Ultrasound

Pierre Bour,[1,2,3,4]* Fabrice Marquet,[1,2,3] Valéry Ozenne,[1,2,3] Solenn Toupin,[1,2,3,5] Erik Dumont,[4] Jean-François Aubry,[6] Matthieu Lepetit-Coiffe,[5] and Bruno Quesson[1,2,3]

Purpose: The therapy endpoint most commonly used in MR-guided high intensity focused ultrasound is the thermal dose. Although namely correlated with nonviable tissue, it does not account for changes in mechanical properties of tissue during ablation. This study presents a new acquisition sequence for multislice, subsecond and simultaneous imaging of tissue temperature and displacement during ablation.

Methods: A single-shot echo planar imaging sequence was implemented using a pair of motion-encoding gradients, with alternated polarities. A first ultrasound pulse was synchronized on the second lobe of the motion-encoding gradients and followed by continuous sonication to induce a local temperature increase in ex vivo muscle and in vivo on pig liver. Lastly, the method was evaluated in the brain of two volunteers to assess method's precision.

Results: For thermal doses higher than the lethal threshold, displacement amplitude was reduced by 21% and 28% at the focal point in muscle and liver, respectively. Displacement value remained nearly constant for nonlethal thermal doses values. The mean standard deviation of temperature and displacement in the brain of volunteers remained below 0.8 °C and 2.5 μm.

Conclusion: This new fast imaging sequence provides real-time measurement of temperature distribution and displacement at the focus during HIFU ablation. **Magn Reson Med 000:000–000, 2017. © 2017 International Society for Magnetic Resonance in Medicine.**

Key words: MRgHIFU; ARFI; thermometry; ablation

INTRODUCTION

MR-guided high intensity focused ultrasound (MRgHIFU) allows for noninvasive ablation of pathological tissue. Current clinical procedures exploit MR images for target delimitation, online thermometry to define a therapy end-point during the ablation, and postablation lesion assessment (1,2). Typically, the principal monitoring parameters are temperature measurement by means of the proton resonance frequency shift (PRFS) (3) along with online thermal dose calculations (4).

During treatment, acoustic characteristics of tissue may change, such as absorption with temperature, tissue elasticity with protein denaturation (5) or, for example, in the presence of cavitation, shock wave (6), or boiling (7). If small bubbles form within the HIFU propagation cone at the patient's body surface during sonication, less acoustic energy is transmitted to the target region, making treatment more difficult to achieve. However, local modifications of tissue characteristics can be exploited to enhance heating efficiency (8) at the focus and to protect tissues located beyond the targeted area (9). Specifically, online rapid monitoring of potential transient changes of tissue acoustic properties during HIFU sonication simultaneously with temperature imaging, may help to improve the safety of the procedure, exploit nonlinear effects (e.g., cavitation) of ultrasound for enhanced heating efficiency and provide additional information on the outcome of the therapy beside conventional thermal dose imaging. The imaging sequence should be fast, allow large spatial coverage and provide a high sonication duty cycle to avoid a loss in heating efficiency.

MR-acoustic radiation force impulse (ARFI) imaging encodes the local displacement of soft tissues induced at the HIFU focal point in the phase image (using a motion-sensitive encoding gradient, MEG) synchronized with short duration ultrasound pulses (10,11). MR-ARFI has been reported to visualize the focal spot location prior to ablation without inducing thermal effects, to compensate tissue aberrations relative to ultrasound propagation in transcranial HIFU ablation (12,13) and to determine the acoustic pressure for exploiting nonlinear effects of HIFU to enhance heating efficiency (8).

MR-thermometry and MR-ARFI imaging are complementary as they are, respectively, sensitive to thermal and mechanical effects. For example, during ultrasonic neuromodulation, nerve conduction blocking has been attributed to a thermal action of ultrasound by some teams (14), whereas other teams attributed it to action of radiation pressure (15) or intramembrane cavitation (16).

[1]IHU Liryc, Electrophysiology and Heart Modeling Institute, Fondation Bordeaux Université, Pessac- Bordeaux, France.

[2]Univ. Bordeaux, Centre de recherche Cardio-Thoracique de Bordeaux, U1045, Bordeaux, France.

[3]INSERM, Centre de recherche Cardio-Thoracique de Bordeaux, U1045, Bordeaux, France.

[4]Image Guided Therapy SA, Pessac, France.

[5]Siemens Healthineers France, Saint-Denis, France.

[6]Institut Langevin, CNRS UMR 7587, INSERM U979, ESPCI ParisTech, Paris, France.

Grant sponsor: French National Investments for the Future Programs ANR-10-IAHU-04 (IHU Liryc) and Laboratory of Excellence ANR-10-LABX-57 (TRAIL), and the research programs ANR-11-TecSan-003-01 (TACIT) and Equipex ANR-11-EQPX-0030 (MUSIC).

*Correspondence to: Pierre Bour, MSc, IHU Liryc, PTIB- Hôpital Xavier Arnozan, Avenue Haut Levêque, 33604 Pessac, France. E-mail: pierre.bour@ihu-liryc.fr

Received 6 May 2016; revised 26 October 2016; accepted 28 November 2016

DOI 10.1002/mrm.26588

Published online 00 Month 2017 in Wiley Online Library (wileyonlinelibrary.com).

Therefore, simultaneous imaging of both temperature and displacement would help to better understand the mechanisms underlying this bioeffect for a given experimental situation.

In the present work, we propose a fast implementation of a simultaneous MR-ARFI-thermometry allowing subsecond multislice imaging of temperature and displacement during HIFU ablation. An MR-ARFI-thermometry sequence has already been proposed (17–19) to visualize focal spot location and to verify the absence of thermal effect before ablation. However, its current implementation has a limited sonication duty cycle to induce thermal necrosis and remains too slow to monitor HIFU ablation. Here, we propose a continuous monitoring of temperature and displacement during a HIFU treatment where we preserved a high sonication duty cycle ($>80\%$) compatible with thermal ablation energy deposition. Additional data reflecting tissue elasticity modifications associated with temperature changes were extracted from displacement measurements.

The method was first evaluated in ex vivo skeletal muscle to demonstrate the benefit and limitations of the technique. Then, in vivo sonications were performed in the liver of pigs to illustrate potential of rapid and simultaneous temperature and displacement monitoring during ablation in a clinically relevant application. Finally, in the perspective of a brain application, a proof of feasibility on two healthy volunteers was conducted to assess the stability of temperature and displacement measurements.

METHODS

All experiments were performed using a 1.5T MR scanner (Magnetom Avanto, Siemens, Erlangen, Germany) with an MR-compatible HIFU platform (Image-guided Therapy SA, Pessac, France). A 256-elements phase array transducer (focal length 13 cm, aperture 13 cm, 1 MHz operating frequency) was used. Each element was driven independently for both amplitude and phase from a programmable generator and associated workstation (Thermoguide^{TM} software, Image Guided Therapy Sa, Pessac, France). The transducer was embedded in a custom-built bed allowing 2D displacement along the horizontal X–Z plane using two MR compatible piezo motors.

A single-shot echo planar imaging (EPI) sequence was modified to insert a bipolar MEG before the echo train (Fig. 1a). The MEG direction was set parallel to the acoustic propagation axis to encode longitudinal tissue displacement induced by HIFU pulses, with adjustable duration (Δ) and amplitude (A, maximal value of 25 mT/m). The polarities of the MEG were alternated during successive dynamic acquisitions to encode displacement into the phase image with either a positive or negative contribution. An analogic synchronization pulse (TTL) was generated by the MR sequence and sent to the trigger input of the HIFU generator. Its timing (δ) could be adjusted relative to the beginning of the second lobe of the MEG. This delay influences the apparent displacement that MEG could encode in the phase image, depending on the tissue displacement time-constant. The HIFU sonication was divided into two independent shots with amplitudes noted S_{ARFI} and S_{THERMO}, respectively. S_{ARFI} overlapped the second lobe of MEG to encode ARFI displacement, whereas S_{THERMO} was applied during the rest of the time sequence except during the first lobe of the MEG, resulting in a large HIFU duty cycle. The duration of the S_{ARFI} pulse was controlled from the Thermoguide^{TM} console and an additional adjustable delay τ (see Figure 1a) was set before the first lobe of the MEG to allow for tissue mechanical relaxation after S_{THERMO} was stopped.

Image Reconstruction & Pipeline

Raw MR data were streamed in real-time to the open source Gadgetron (20) framework for image reconstruction. The reconstruction process included EPI (ghost correction using three acquisition lines of central k-space line) and parallel image reconstruction with Grappa acceleration (factor = 2). Magnitude and phase images were transferred by TCP/IP to Thermoguide^{TM} for online computation and display of temperature images and displacement maps using a customized software.

For each slice the pipeline: (i) computed the temporal standard deviation in each pixel from phase data over the first 10 acquisitions in the time series; (ii) automatically generated an image mask to exclude pixels with a phase standard deviation higher than 0.5 rad; (iii) performed a temporal phase unwrap of phase data over the computed mask.

Computation of Temperature and Displacement

With the proposed sequence, both displacement (D) and temperature (T) were encoded into the phase image. Therefore, a second order finite development of the phase φ led to the following equation:

$$\varphi = \varphi_{ref} + \alpha_T.T + \alpha_D.D + \beta_T.T^2 + \beta_D.D^2 + \theta.D.T \quad [1]$$

with (α_T,α_D,β_T,β_D,θ) constants and φ_{ref} a reference phase

Anterior works (3,12) have shown that the phase variation induced by temperature or displacement taken independently was linear, thus β_T and β_D can be considered negligible in a first approach. In Equation [1], $\alpha_T = \gamma.\alpha.TE.B0$ and $\alpha_D = \gamma.A.\Delta$, where $\gamma = 267.51\ 10^6$ rad.s^{-1}.T^{-1} was the gyromagnetic ratio, $\alpha = -0.0094$ ppm.°C^{-1} (21) the PRFS constant, TE the echo time, B0 = 1.5T the static magnetic induction, Δ was the duration of the MEG, and A its amplitude.

Assuming that θ, the coefficient of second-order mixed partial derivatives of temperature and displacement, can be neglected, Equation [1] became:

$$\varphi = \varphi_{ref} + \alpha_T.T + \alpha_D.D. \quad [2]$$

The sequence described in this manuscript used an alternating MEG ($A = (-1)^i|A|$ where i was the dynamic acquisition number in the time series and $\alpha_D = (-1)^i.\gamma.|A|.\Delta$). Therefore, the average temperature $\bar{T}_i$ and displacement $\bar{D}_i$ on two successive dynamic acquisition was computed by summing and subtracting two consecutive phase images:

$$(\varphi_i^+ - \varphi_{ref}^+) + (\varphi_{i-1}^- - \varphi_{ref}^-) = \gamma.\alpha.TE.B0.(T_i + T_{i-1}) + (-1)^i.\gamma.|A|.\Delta.(D_i - D_{i-1}) \quad [3]$$

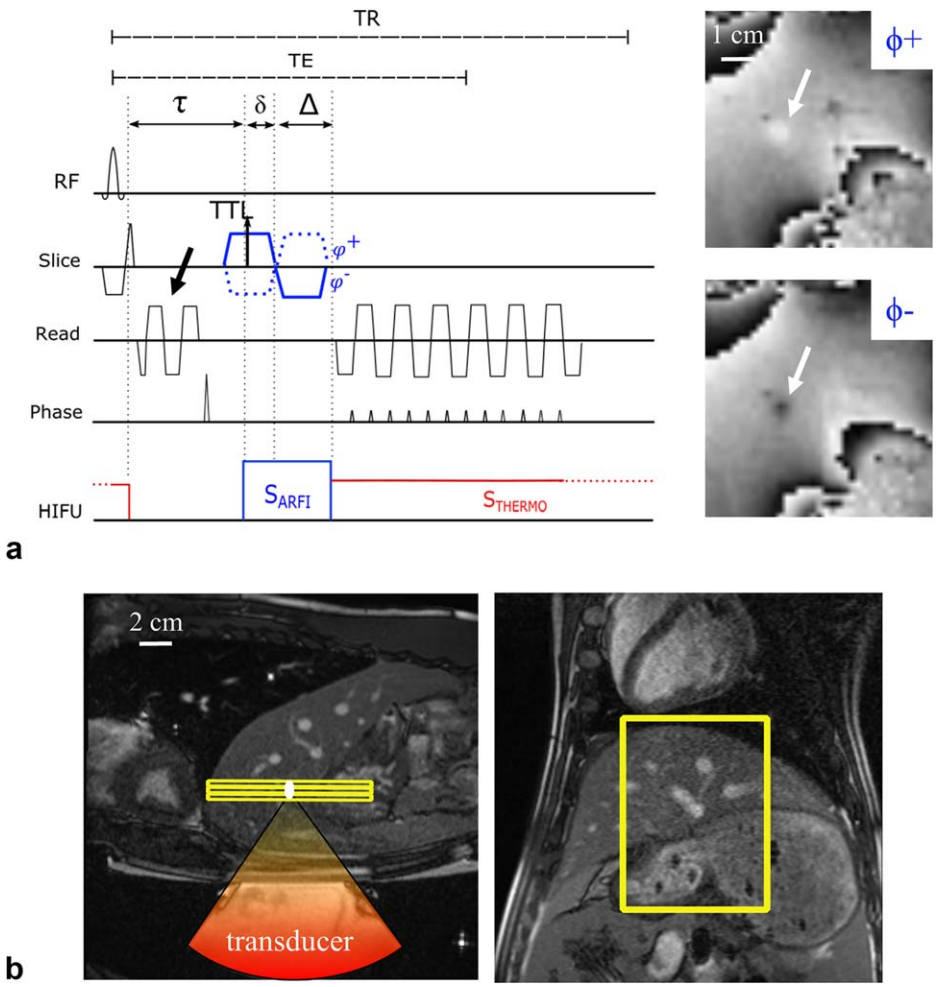

FIG. 1. Description of the MR-ARFI-thermometry method. **a**: Schematic of the single-shot echo planar imaging MR-ARFI-thermometry sequence integrating MEG (in blue) with alternating polarities (φ^+ and φ^-) to encode both temperature and ARFI displacement in the phase of the reconstructed MR image. Black arrows show zero k-space lines used for EPI phase correction. Ultrasound sonications (S_{ARFI}) and (S_{THERMO}) are represented in the bottom line. The TTL arrow indicates the timing of the output synchronization signal from the MR acquisition sequence used for triggering the (S_{ARFI}) pulse of the HIFU generator. δ and Δ (see the Methods section for details) represent the adjustable offset of the TTL signal relative to the beginning of the second lobe of the MEG gradient and the duration of this lobe, respectively. Images on the right display representative phase images for alternative MEG polarities, with the focal spot location indicated by arrows. **b**: 2D balanced-SSFP images acquired in sagittal (left) and coronal (right) orientations in vivo on a pig for localization of HIFU transducer, targeting of the beam into the liver and positioning of the acquisition slices for the sequence presented in (a). Yellow lines represent the three slices, centered on the HIFU focal location. The ultrasound cone is represented on the sagittal slice. The white horizontal scale indicated on each image represents 2 cm.

$$(\varphi_i^+ - \varphi_{ref}^+) - (\varphi_{i-1}^- - \varphi_{ref}^-) = (-1)^i.\gamma.|A|.\Delta.(D_i + D_{i-1}) + \gamma.\alpha.TE.B0.(T_i - T_{i-1}) \quad [4]$$

$$\bar{T}_i = \frac{T_i + T_{i-1}}{2} = \frac{(\varphi_i^+ - \varphi_{ref}^+) + (\varphi_{i-1}^- - \varphi_{ref}^-)}{2.\gamma.\alpha.TE.B0} - \varepsilon_T \quad [5]$$

$$\bar{D}_i = \frac{D_i + D_{i-1}}{2} = (-1)^i \frac{(\varphi_i^+ - \varphi_{ref}^+) - (\varphi_{i-1}^- - \varphi_{ref}^-)}{2.\gamma.|A|.\Delta} - \varepsilon_D \quad [6]$$

From Equations [5] and [6], the errors in temperature (ε_T) and displacement (ε_D) were proportional to the temporal derivatives of displacement and temperature curves, respectively:

$$\varepsilon_T = \frac{\alpha_D}{2.\alpha_T}(D_i - D_{i-1}) \quad [7]$$

and

$$\varepsilon_D = \frac{\alpha_T}{2.\alpha_D}(T_i - T_{i-1}) \quad [8]$$

ε_T and ε_D led to artifact at the onset and offset of HIFU sonication where the temperature and displacement derivatives were maximum.

Thermal dose was computed from temperature images using the Sapareto and Dewey (22,23) algorithm with a threshold for the lethal thermal dose (LTD) of 240 min at 43 °C. For in vivo experiments, the rectal temperature measured by an optical probe served as the reference temperature for thermometry.

Ex Vivo Experiments

Ex vivo validation was performed on 10 fresh ex vivo pig muscle samples. A Plexiglas tank filled with deionized water was thermo-regulated at 37 °C. The sample was positioned inside the water tank in a plastic box on top of the ultrasound transducer. Millar membranes (50 μm thick, smaller than 1/30 of the ultrasonic wavelength) were glued to the base of the plastic box and water tank to ensure ultrasound wave propagation from the transducer toward the sample. Two six-element MR coils were positioned laterally to the Plexiglas tank and

an additional single loop coil (19 cm in diameter) was positioned on top of the plastic box containing the muscle sample.

Animal Preparation

In vivo validation was performed on the liver of three pigs (Large White x Landrace, ~40 kg). The protocol was approved by the local Animal Research Ethics Committee "CEEA50" according to the European rules for animal experimentation. After premedication of pigs with ketamine (20 mg.kg^{-1}) and acepromazine (1 mg.kg^{-1}) by an intramuscular injection, the induction of anesthesia was realized with intravenous (IV) bolus of ketamine (15 mg.kg^{-1}) and midazolam (1.5 mg.kg^{-1}). This step was followed by intubation, ventilation and shaving of the thoraco-abdominal region. Depilatory cream (Veet, Reckitt Benckiser, Slough, UK) was used to remove residual hair in the sonicated area. The animal was placed in the prone position on the MR-HIFU platform to avoid transcostal sonication. Figure 1b shows the animal positioning with respect to the HIFU transducer. The animal was assisted for ventilation (AESTIVIA, General Electric, Fairfield, CA) and maintained under general anesthesia with continuous IV injection of ketamine and midazolam (40 mg.kg^{-1}.h^{-1} and 2 mg.kg^{-1}.h^{-1}, respectively).

ECG and arterial pressure were recorded during the procedure. MR data was acquired using two 16-element antennas positioned laterally to the thorax and a 19 cm loop coil was positioned underneath the animal on top of the HIFU device. After completion of the treatment, the animal was euthanized with an IV injection of Dolethal (Vetoquinol, Lure, France), until complete cardiac arrest was attested from the ECG trace. The liver was extracted surgically for gross pathology examination.

Experimental Protocol

The procedure followed these steps:

1. Localization of the organs relative to the transducer position using a 2D multi-slice balanced-SSFP sequence: FOV = $250 \times 250\,mm^2$, TR/TE/FA = 486 ms/1.36 ms/80°, $1 \times 1 \times 3\,mm^3$ voxel size, with a bandwidth of 1495 Hz per pixel. 40 slices on each orientation centered at the focus were acquired. From this stack of images, a target region was defined on the planning console of the HIFU control software.
2. Optimization of the Experimental Parameters. The apparent displacement derived from MR phase image may be influenced by experimental choices of δ (delay related to time for tissue to reach a steady state during S_{ARFI}) and τ (delay postsonication S_{THERMO} to let tissue relax toward its initial position before encoding next displacement with S_{ARFI}). Thus, a preliminary batch of experiments was conducted in ex vivo muscle to optimize these parameters. The proposed sequence was ran with the following acquisition parameters: one coronal slice with fat saturation, FOV = $92 \times 147\,mm^2$, TR/TE/FA = 800 ms/29 ms/45°, voxel size = $2.1 \times 2.1 \times 5\,mm^3$, with a bandwidth of 1500 Hz per pixel, Grappa acceleration (factor = 2), A = 25 mT/m, Δ = 5.3 ms.

Tuning of Delays δ and τ

A first series of measurements was performed to quantify the influence of δ. For this purpose, S_{THERMO} was set to 0 and displacement and temperature were monitored for different values of δ ranging from 0 to 3 ms in steps of 1 ms. Each condition was ran with 50 repetition times to compute mean ± SD values of apparent displacement at the focus and to plot these values as a function of δ. The value of δ leading to the maximal apparent displacement was considered to be the optimal choice.

A second series of experiments were performed to measure the optimal value of τ, with δ previously determined and [S_{ARFI}, S_{THERMO}] = [198, 198] W acoustic power, while reducing τ from 50 ms to 10 ms. A sonication of 5 s was performed for each delay, interleaved with a cooling period (~ 10 s) to avoid excessive increases in temperature. Mean ± SD values of apparent displacement over 10 repetitions were computed and plotted as a function of τ.

3. Calibration of ARFI measurement without heating ($S_{THERMO} = 0$) allowed to define the practical amplitude S_{ARFI} required to encode displacement and to precisely locate the focal spot location within the targeted region. During this step, 3 to 5 shots with incremental S_{ARFI} amplitude were performed. The sequence was ran with the following parameters: (i) Ex vivo, three coronal slices with fat saturation, FOV = $92 \times 147\,mm^2$, TR/TE/FA = 266 ms/29 ms/45°, voxel size = $2.1 \times 2.1 \times 5\,mm^3$, with a bandwidth of 1500 Hz per pixel, Grappa acceleration (factor = 2), A = 25 mT/m, Δ = 5.3 ms, and δ = 3 ms for the MEG; (ii) In vivo, three slices in the coronal plan with fat saturation and saturation slabs surrounding the FOV in the phase direction, FOV = $156 \times 170\,mm^2$, TR/TE/FA = 333 ms/28 ms/50°, $2.3 \times 2.3 \times 5\,mm^3$ voxel size, with a bandwidth of 2003 Hz per pixel, Grappa acceleration (factor = 2), A = 25 mT/m, Δ = 5.3 ms, and δ = 3 ms for the MEG. During sonication, a breath hold of 50 s was maintained to avoid respiratory motion.

4. Ablation procedure with $S_{THERMO} > 0$ and S_{ARFI} determined in step 3, using identical MR acquisition parameters. Temperature and displacement maps were overlaid in real-time on magnitude images, together with temporal evolution of temperature, displacement and thermal dose values in selected pixels located in heated/non heated regions. Three points of interest were identified on the displacement curves to quantify the elasticity contrast: the initial, the maximal and the final value of displacement. The initial value was determined as the first measurement of displacement after the artifact at the onset of HIFU emission.

Volunteer Study

Two healthy volunteers were informed about the protocol and consented to be included in the study. They were included in the protocol to assess the mean standard deviation of temperature and displacement measurements on the brain with the proposed sequence. The

protocol was performed using six-element brain array coils where 10 slices without spacing between slices were acquired at 1 Hz for 3 min 20 s (200 dynamics acquisition) with FOV = $156 \times 170\,mm^2$, TR/TE/FA = 100 ms/28 ms/60°, $1.6 \times 1.6 \times 3\,mm^3$ voxel size, with a bandwidth of 1447 Hz per pixel with Grappa acceleration (factor = 2), A = 25 mT/m, $\Delta = 5$ ms for the MEG. The orientation of MEG was craniocaudal for all slice orientations.

For temperature data analysis, a spatiotemporal baseline correction proposed in a previous publication (24) was performed to correct for phase drift during long acquisitions. Mean standard deviation of temperature and displacement images were then computed and analyzed in a region of interest (ROI) covering the entire brain and in a smaller ROI corresponding to accessible regions of the brain from current clinical HIFU devices. The whole brain ROI was automatically computed on modulus, averaged over all dynamics, taking into account pixels with values above 25% of mean maximum intensity. This was performed on each slice for each orientation. Displacement and temperature distrubitions were analyzed in a Box and Whisker plot for each volunteer.

RESULTS

Figure 2a shows the apparent displacement for the pixel at the focus measured in ex vivo muscle for $\delta = 0$, 1, 2, and 3 ms. The curve displays a progressive increase in apparent displacement from $\delta = 0$ ms ($12.3 \pm 1.4\,\mu m$) with a plateau near 30 μm reached for δ around 2 to 3 ms. Thus, δ was kept at 3 ms for all ex vivo experiments on muscle. Identical value was used during in vivo for experiments on pig liver based on previously published data (18) leading to similar observation with a different acquisition sequence.

Figure 2b shows the apparent displacement in the pixel at the focus after a 5-s sonication interleaved with a cooling period of 10 s, for different values of τ. Similar values were observed for each experimental condition with a mean apparent displacement around 30 μm, identical to the values reported in Figure 2a in the absence of S_{THERMO}. A maximal temperature increase was found below 7 °C (data not shown), indicative of negligible accumulated thermal dose and absence of thermal damage. A value of 10 ms after S_{THERMO} was thus considered sufficient to ensure full relaxation of tissue before next encoding of S_{ARFI} at the following dynamic acquisition in the time series.

Figure 2c shows sonication performed in ex vivo pig muscle with simultaneous estimation of temperature and displacement. Artifacts (orange squares) at the beginning and completion of the HIFU sonication, resulted from uncompensated MEG encoding in the iterative subtraction of phase images (see Eqs. [5] and [6]) at these time points.

Figure 2d displays the computed error in temperature and displacement (according to Eqs. [7] and [8]) from the same experiment. The standard deviation of temperature estimation error before and during sonication were 0.33 °C and 0.30 °C, respectively. Displacement estimation led to a standard deviation error of 1.0 μm before sonication and 1.0 μm during sonication.

Figure 3 presents typical results of the calibration step obtained ex vivo and in vivo. The displacement and associated temperature increase for the pixel located at the focal spot are displayed for four different acoustic powers applied to the HIFU transducer (Fig. 2a). The standard deviation of the displacement measured prior to sonication was 1.2 μm ex vivo and 1.4 μm in vivo. Ex vivo, we measured 6, 12, 19, and 32 μm for acoustic power values of 53, 74, 158, and 198 W, respectively. In vivo, we measured 9, 15, 21, and 52 μm maximal displacement for acoustic power values of 99, 158, 198, and 470 W, respectively. Displacement curves as a function of acoustic power were fitted with a linear function to determine the slope (see values on the curves in Figure 3c). Maximal temperature increase during this procedure was 2.6 ± 0.3 °C ex vivo and 2.1 ± 0.4 °C in vivo. In Figure 3b, displacement and temperature maps were overlaid on magnitude images. Ex vivo and in vivo, the spatial distribution of the temperature remained localized at the focus and did not exceed 3 °C for the hottest pixel demonstrating that tissue was not significantly heated during this procedure.

Figure 4 displays representative results of HIFU ablation for the ex vivo and in vivo experiments with the proposed MR-ARFI-thermometry monitoring method. The values of [S_{ARFI}, S_{THERMO}] were [198, 128] W acoustic for the ex vivo muscle experiment (two minutes sonication) and [470, 470] W in the liver of pig (30-s sonication). Local temperature increase and displacement were visible in both images (Fig. 4a) at identical spatial locations. In both cases, the temperature increase was associated with a decrease in displacement (Fig. 4b). Maximal temperature increases were 15 ± 0.4 °C in the muscle and 26 ± 0.5 °C in the liver, respectively. During sonication, initial, maximal and final displacement values were 30 μm, 32 μm, and 23 μm in the muscle and 41 μm, 80 μm, and 31 μm in the liver.

Figure 5a presents comparative results of representative experiments including the temperature, cumulative thermal dose and the displacement curves at the focus. For both ex vivo and in vivo conditions, two examples of results of HIFU sonication are displayed with/without reaching the LTD. When the LTD threshold could not be reached, the maximal displacement remained nearly constant, whereas it decreased when the LTD was reached. In some experiments, the displacement at the beginning of the sonication displayed a progressive increase before reaching the thermal dose (see Figures 5b,d).

Table 1 summarizes the results for all the sonications. The maximal variation of the displacement remained below 5% for all sonications performed with insufficient accumulated thermal dose (maximal temperature increase below 16 °C), whereas it displayed a relative decrease of $21 \pm 7\%$ (ex vivo) and $28 \pm 6\%$ (in vivo) for sonications in which the LTD threshold was reached.

Results on Volunteers

Figure 6 displays results of the temperature and displacement maps obtained on the brain of volunteer #2 with the

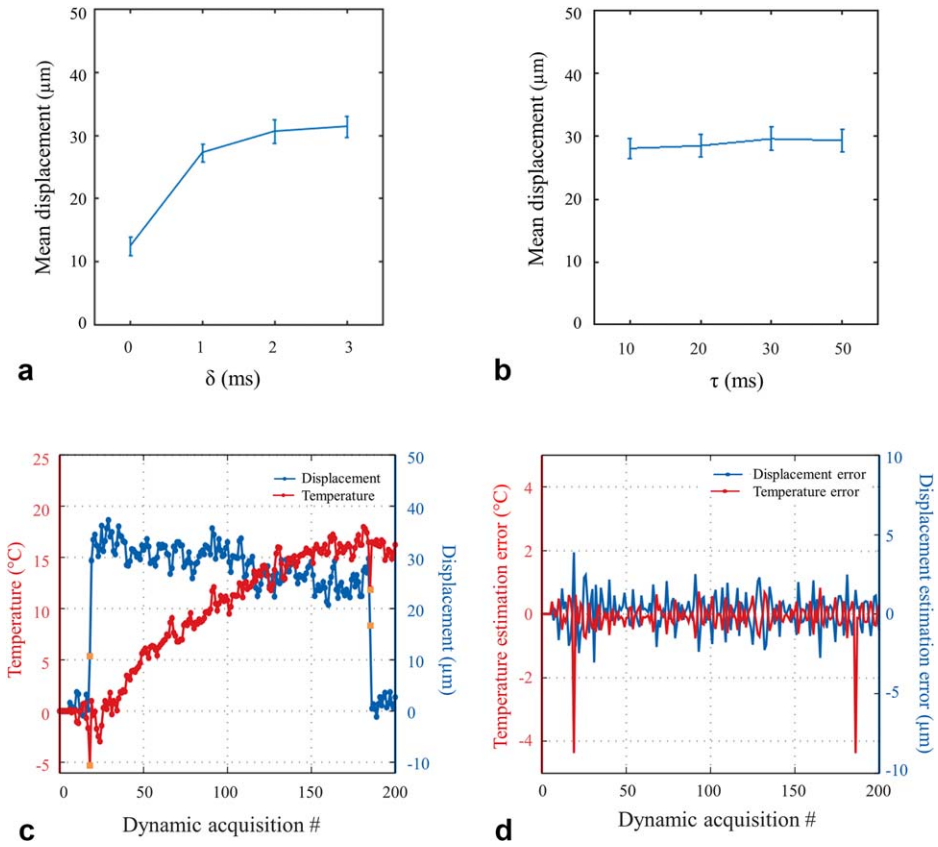

FIG. 2. Sequence parameter optimization, representative results in ex vivo muscle and errors in temperature and displacement measurement. **a**: Mean ± SD of tissue apparent displacement at the focus as a function of δ, using $[S_{ARFI}, S_{THERMO}] = [198, 0]$ W. Curves were computed from 50 independent measurements. A plateau of ~30 μm is reached at δ = 2-3 ms. **b**: Mean ± SD of tissue apparent displacement at the focus as a function of τ, using $[S_{ARFI}, S_{THERMO}] = [198, 198]$ W. For these experiments, δ was set to 3 ms and curves were computed from 10 independent measurements consisting of 5 s sonication duration interleaved with a 10 s cooling period. A mean displacement of around 30 μm (identical to the value reported in (a) when $S_{THERMO} = 0$) is observed whatever the value of τ. Maximal temperature remained below 7 °C (not shown). **c**: Representative result of temperature and displacement curves obtained in ex vivo pig muscle with the proposed sequence. Sonication duration was 120 s, with δ = 3 ms, τ = 10 ms and $[S_{ARFI}, S_{THERMO}] = [198, 128]$ W. Orange squares represent artifacts in temperature and displacement estimates resulting from the data processing (see Eqs. [5] and [6]), when ultrasound is turned on and off, respectively. **d**: Computation of the error in temperature and displacement using Equations [7] and [8], from the experimental data plotted in (c). Standard deviation of temperature and displacement are 0.33 °C and 1.0 μm before sonication and 0.30 °C and 1.0 μm during sonication (excluding times points when ultrasound is turned on/off), respectively.

proposed sequence. A volume of 230x160x30 mm^3 for each orientation was acquired every second. In the ROI covering the whole brain the median of the mean standard deviation maps of the temperature and displacement in coronal, sagittal and transversal orientations were 0.7 °C and 2.5 μm, 0.7 °C and 1.8 μm, 0.6 °C and 2.2 μm, respectively. In the ROI located in the center of the brain, the mean standard deviation values of the temperature and displacement in coronal, sagittal and transversal orientations were 0.7 °C and 2.4 μm, 0.8 °C and 2.1 μm, 0.7 °C and 2.2 μm, respectively. The box and whisker plots of the distribution of temperature and displacement values in the centered ROI showed that 75% of the pixels display a temperature and displacement mean standard deviations below 1 °C and 3 μm in coronal orientation, 0.9 °C and 2.6 μm in sagittal orientation and 0.7 °C and 2.8 μm in transversal orientation, respectively.

DISCUSSION

The hybrid MR-ARFI-thermometry sequence and the associated posttreatment allow real-time visualization of temperature and displacement with a repetition time below 100 ms and a spatial resolution of $2.3 \times 2.3 \times 5\ mm^3$ in vivo. Note that although the tissue displacement was encoded into the MR phase image using the MEG, the computed value of displacement has to be considered as an apparent displacement, because it is averaged over the voxel size and that its value may also be affected by sub optimal choice of δ and τ. For this purpose, an experimental approach was proposed to optimize these parameters, as illustrated in Figure 2.

In our experimental conditions the error in the estimation of temperature and displacement (see equation [7] and [8]) were $|\frac{\alpha_D}{2\alpha_T}| = 0.16\ °C.\mu m^{-1}$ and $|\frac{\alpha_T}{2\alpha_D}| = 1.5\ \mu m.°C^{-1}$

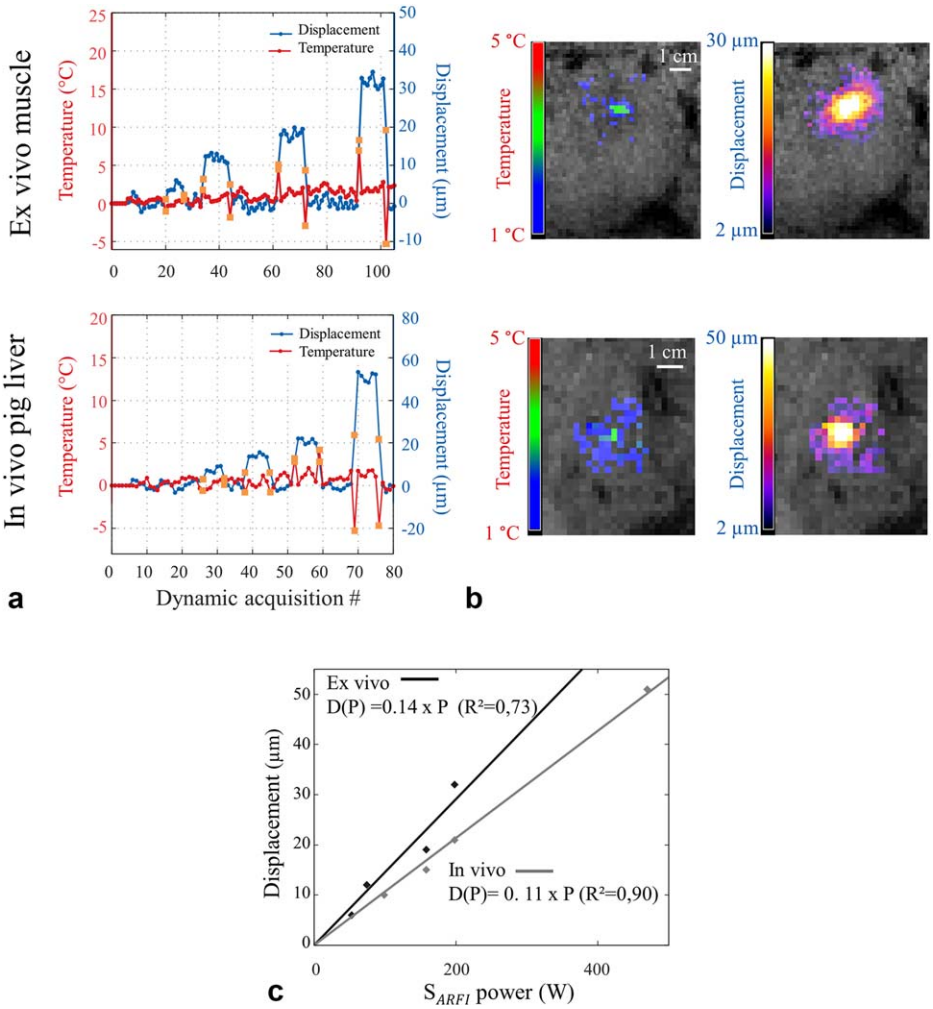

FIG. 3. Representative results of the calibration step (S_{THERMO}=0) from ex vivo and in vivo experiments. **a**: Temporal evolution of displacement (blue curve) and temperature (red curve) in the pixel located at the HIFU focal point. Four sonications were performed with S_{ARFI} of 53, 74, 158 and 198 W ex vivo and 99, 158, 198 and 470 W in vivo, respectively. Orange squares represent artifacts in temperature and displacement estimates resulting from the data processing (see Eqs. [5] and [6]), when ultrasound is turned on and off, respectively. **b**: Corresponding temperature and displacement images overlaid on magnitude images for the fourth HIFU shot. Temperature and displacement scales are indicated on each graph. Horizontal white bar on temperature images represent 1 cm. **c**: Plots of displacement measured at the focus as a function of S_{ARFI} for both experiments displayed in (a). Continuous lines represent the result of the linear fit of both curves, with slope and R^2 values indicated on each curve.

ex vivo, and $|\frac{\alpha_D}{2\alpha_T}| = 0.17\,^{\circ}\mathrm{C}.\mu\mathrm{m}^{-1}$ and $|\frac{\alpha_T}{2\alpha_D}| = 1.5\,\mu\mathrm{m}.^{\circ}\mathrm{C}^{-1}$ in vivo, respectively. The standard deviation of the error in temperature and displacement estimates (see Figure 2d) showed similar values before and during sonication. These values depended on the experimental noise in phase images and on the proposed processing method. The latter contribution can be minimized by rapid sampling to avoid important variations of temperature and displacement between successive measurements (see Eqs. [7] and [8]). This justifies the use of a rapid imaging sequence based on a single-shot EPI acquisition. In vivo on the liver of pig, only a limited period of acquisition was available (50 s) due to apnea. The ablation process was required to be quicker (30 s) than for sonications performed in ex vivo muscle. Hence, signal-to-noise ratios of temperature and displacement curves were lower than for the results obtained in ex vivo muscle.

However, with the proposed MEG combination of parameters ($\Delta = 5.3$ ms and $A = 25$ mT/m), the displacement sensitivity was $14.1\,\mu\mathrm{m}.\mathrm{rad}^{-1}$ and standard deviation of temperature and displacement measurements were found to be sufficient for visualizing the focal spot ex vivo in skeletal muscle and in vivo in pig livers.

In the proposed method, the loss in sonication duty cycle was limited ($\sim$ 15%) and corresponded to the dead time at the beginning of the sequence to allow the tissue to mechanically relax toward its initial position before the next ARFI displacement encoding. Results obtained during this study indicate that energy deposition under these experimental conditions was sufficient to create thermal lesions in muscle and liver and to quantify simultaneously tissue mechanical changes at the focal point through apparent displacement variations, temperature distribution in the heated area and thermal dose evolution. Although the principle of simultaneous measurement of displacement and temperature has already been reported (17,18), it remained limited to the assessment of temperature increase during focal spot localization, without adjunction of a second HIFU pulse dedicated to thermal ablation. Moreover, these acquisition sequences were segmented EPI, which required several repetitions to reconstruct one image. Mougenot et al (17) reported an improvement of 41% in temperature and displacement measurements without alternating MEG polarity, but using a variable trigger delay for sonication, synchronized alternatively on the first or second lobe of MEG. Such a method may also be implemented with a single-shot EPI. Although voxel size reported in Mougenot et al. (17) and Auboiroux et al (18) was smaller in the liver using a segmented EPI acquisition

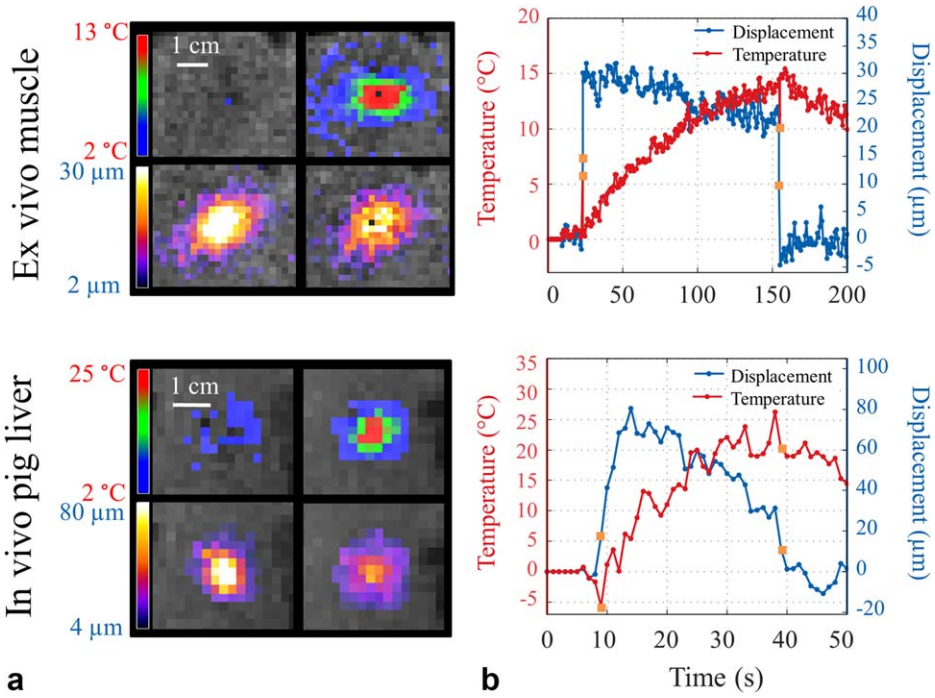

FIG. 4. Results of representative ex vivo and in vivo experiments during HIFU sonication ($S_{THERMO} > 0$). **a**: Temperature (top row) and displacement (bottom row) maps overlaid to magnitude images obtained at the beginning (left column) and at the end (right column) of the HIFU sonication, in ex vivo muscle and in vivo in the liver of one pig. Color bars indicate temperature and displacement scales and the white horizontal bar on temperature images represent 1 cm. **b**: Temporal evolution of the temperature and displacement in the hottest pixel. HIFU sonication lasted 2 min for ex vivo muscle experiment with [S_{ARFI}, S_{THERMO}] of [198, 128] W. For in vivo experiment on the liver of a pig performed under apnea, the sonication duration was 30 s with [S_{ARFI}, S_{THERMO}] of [470, 470] W. Orange squares represent artifacts in temperature and displacement estimates resulting from the data processing (see Eqs. [5] and [6]), when ultrasound is turned on and off, respectively.

sequence with respiratory gating at 3T, the spatial resolution in this study was considered sufficient to monitor temperature and displacement changes during HIFU sonication. Displacement amplitudes found ex vivo on pig muscle (~40 µm) are in agreement with those from Mougenot et al (17). Auboiroux et al (18) reported from in vivo pig liver, a lower displacement (less than 15 µm) during a transcostal sonication, whereby a significant portion of acoustic power was absorbed by the rib cage. In our experimental conditions, displacement estimations were higher. However, Figures 3b,c showed a linear relationship between displacement and acoustic power in the range of acoustic powers used in this study. Thus, induction of nonlinear effects that could interfere with displacement measurement is unlikely under these experimental conditions.

The proposed faster implementation enables acquisition of several slices in a subsecond temporal resolution, calibration of S_{ARFI} with negligible acoustic energy deposition (attested by absence of heating, see Figure 3) and provides full flexibility on the balance between displacement sensitivity and acoustic energy deposition for ablation. In the present work, sonication of S_{ARFI} during the ablation procedure could have been maintained before and after $S_{THERMO} > 0$ for continuous monitoring of displacement but this was not implemented for practical reasons. Our results are in agreement with recent studies on elasticity monitoring during HIFU ablation using either ultrasound shear wave imaging (SWI) (25) or harmonic motion imaging (26). Hou et al (27) observed a decrease of displacement and Arnal et al (25) observed an increase of shear modulus for temperatures higher than 55 °C.

The overall decrease of displacement found in this study could be attributed to increased shear modulus during tissue denaturation (qualitative elasticity contrast). Another driving factor of focal displacement change is the potential variation of attenuation with temperature. A previous study (28) reported that attenuation is increasing with temperature (51% attenuation increase for temperature increase from 37 °C to 65 °C), which would result in an apparent increase of displacement at the focal point. Such an increase in displacement could be observed at the beginning of thermal accumulation and before reaching the lethal thermal dose on Figures 5b,d for in vivo and ex vivo experiments. Values are consistent with the linear slope reported by Arnal et al (25) below 50 °C, using shear wave imaging.

Such an increase in displacement may also be attributed to rapid boiling at the focus that would locally modify tissue stiffness, as reported by Khokhlova et al (29) and Elbes et al (7). However, Khoklova et al reported that boiling can occur in a few milliseconds although the increase in displacement observed in Figure 5 lasts several seconds. Moreover, as already mentioned above, nonlinear effects are unlikely to occur in our experiments. Addition of backscattered ultrasound signal measurement during sonication to monitor nonlinear ultrasound effects may provide additional information. Qualitative gross pathology observations of the tissue was performed to verify the presence of thermal lesion, but no inference of lesion extent based on displacement variation has been made in this study that focuses on presenting a new MR acquisition method. Further studies could encompass mapping displacement variation using beam steering capabilities of the HIFU probe then correlating measured lesion extent with postablation imaging.

This single-shot EPI ARFI-thermometry sequence allows rapid focal spot localization using only two HIFU

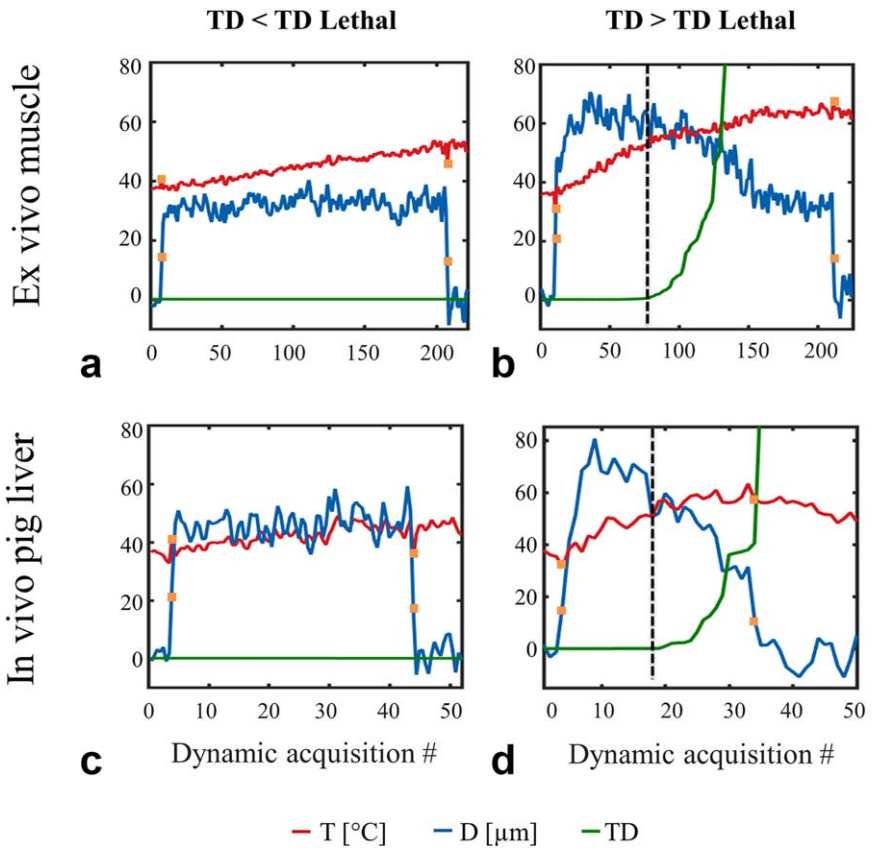

FIG. 5. Examples of temporal evolution of displacement (D), temperature (T) and accumulated thermal dose (TD) for sonications performed ex vivo (muscle) and in vivo (pig liver). For each graph, temperature (red), displacement (blue) and thermal dose (green) curves are plotted as a function of time. Top row shows representative results obtained on the muscle and bottom row shows representative results in the liver of pig. Graphs in the left column display results where the thermal dose (TD) did not reach the lethal value (LTD), and graphs in the right column display results where the lethal thermal dose was reached (TD > LTD). Orange squares represent artifacts in temperature and displacement estimates resulting from the data processing (see Eqs. [5] and [6]), when ultrasound is turned on and off, respectively. **a**: Example of a sonication in muscle resulting in insufficient heating to reach the lethal thermal dose (TD < LTD). **b**: Example of a sonication in muscle resulting in sufficient heating to reach the lethal thermal dose (TD > LTD). **c**: Example of a sonication in pig liver resulting in insufficient heating to reach the lethal thermal dose (TD < LTD). **d**: Example of a sonication in pig liver resulting in sufficient heating to reach the lethal thermal dose (TD > LTD).

pulses, as the first measurement correspond to the artifact at the onset of HIFU sonication. However, the resulting energy deposition remains limited, as illustrated by negligible temperature increases observed in Figure 3. As such, it may provide a safer way to identify the effective sonication beam's location in the targeted area than the usual methods relying on the observation of local temperature increase during pre-intervention sonication performed at low energy.

MRgHIFU brain therapies are increasingly used for new clinical applications and may benefit from improved temporal and spatial quantitative monitoring, as current monitoring methods are restricted to a single slice with limited spatial resolution and temporal update (30–32). Using our sequence with 10 slices per second and taking advantage of the higher signal-to-noise ratio and the longer T2* in the brain, the spatial resolution of the temperature and displacement images were improved, with a resulting voxel dimension ($1.6 \times 1.6 \times 3\,mm^3$) in the same range as the focal spot dimension of current clinical HIFU devices. On Figure 6c, the mean standard variation of displacement was below 2.5 μm. Experiments performed in ex vivo human skull (33) showed displacements over 20 μm using phase aberration corrections methods.

Although direct comparison of displacement on in vivo and ex vivo brain tissue must be taken with care, our results in terms of standard deviation of displacement in the brain open promising perspectives for the application of this method for clinical treatment. Thus, mechanical changes associated with temperature

Table 1
Maximal Temperature, Accumulated Thermal Dose, and Tissue Displacement at the Focus for Experiments Performed In Ex Vivo Pig Muscles and In Vivo Pig Livers[a]

	Ex vivo pig muscle		In vivo pig liver	
	TD > LTD N = 11	TD < LTD N = 3	TD > LTD N = 8	TD < LTD N = 2
TD/LTD ratio (mean ± SD)	60 ± 23	0.7 ± 0.2	20 ± 10	0.5 ± 0.3
Maximum temperature increase (°C)	20 ± 6	14 ± 4	26 ± 7	16 ± 1
From maximal to final displacement decrease (μm)	21 ± 10	4 ± 3	35 ± 14	3 ± 4
From maximal to final relative displacement decrease (%)	30 ± 6	3 ± 2	39 ± 10	5 ± 3
From initial to final displacement decrease (μm)	17 ± 8	4 ± 3	25 ± 9	3 ± 4
From initial to final relative displacement decrease (%)	21 ± 7	3 ± 2	28 ± 6	5 ± 3

[a]Data are sorted as a function of the accumulated thermal dose (TD), depending on whether it reached or not the lethal thermal dose (LTD) value. The ratio TD/LTD, maximal temperature increase, absolute and relative displacement decreases are reported as mean ± SD values. N values indicated on top of each column are the number of sonications for each condition.

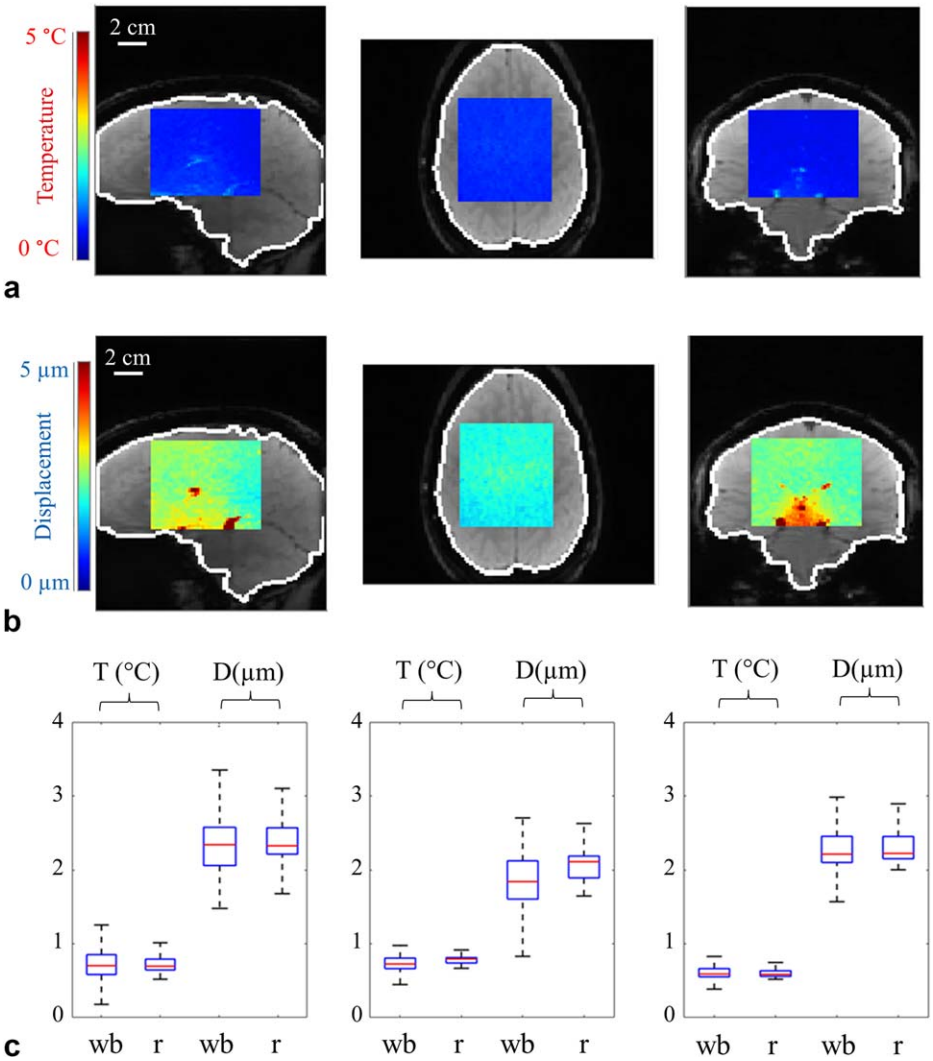

FIG. 6. Standard deviation maps of temperature and displacement obtained on one volunteer. **a**: Central slices of the stack of 10 slices acquired in sagittal (left), transverse (center) and coronal (right) orientations. Temperature standard deviation (color code is indicated on the right) is displayed in the central ROI (see the Methods section for details) overlaid on time-averaged magnitude images. The contour of the ROI surrounding the whole brain is indicated by white pixels on each slice. **b**: Displacement standard deviation (color code is indicated on the right) in identical ROIs to images displayed in (a). **c**: Box and whiskers plots of temperature and displacement distributions with thresholds of 10%, 25% (bottom of the blue box), median value (horizontal red line), 75% (top of the blue box) and 90%. On horizontal axis of each graph, "wb" stands for whole brain ROI [white contour in (a)] and "r" for the central ROI [displayed in (a)]. Data analysis include all data from both volunteers. Horizontal white bars on the images represent 2 cm.

increase during HIFU ablation could be monitored more precisely. Moreover, current clinical brain therapy MR-HIFU devices operate at 3T and are equipped with stronger gradients, which could potentially provide better spatial resolution on both temperature and displacement images and more accurate measurements, thanks to an increased signal-to-noise ratio.

Several studies have reported the added value of exploiting nonlinear acoustic propagation (e.g., cavitation, boiling) to increase heating efficiency at constant acoustic energy and to protect organs located in the far field of the HIFU beam (9,34). The present method would allow rapid calibration of the HIFU power and slice position for exploiting such effects on the liver, as suggested by Ramaekers et al (6). In addition, this study proposed to use a respiratory gated sonication which overcomes the use of real-time motion compensation strategies on temperature and displacement images, although these methods have only been evaluated in preclinical studies where breathing was fully controlled.

The proposed method may still benefit from further improvements. Particularly, earlier no motion and susceptibility-related compensation was incorporated in the treatment pipeline, as the main objective of the study was to describe a new MR-ARFI-thermometry acquisition sequence and provide experimental data illustrating the additional information given by the method for monitoring HIFU ablation in soft tissue. For in vivo experiments in the liver, displacement of the target relative to the HIFU probe was suppressed by breath holding. However, several correction methods for magnitude and phase images are available to compensate motion and associated susceptibility artifacts (35) and could be applied to allow free breathing temperature and displacement imaging on mobile organs, together with real-time locking of the HIFU beam on the target. In our experiments, the spatial resolution was experimentally adjusted as a tradeoff between signal-to-noise ratio, echo train duration and T2* decay, which resulted in acceptable standard deviation on both temperature and displacement measurements.

CONCLUSIONS

This study proposes a new rapid MRI sequence for subsecond, multi-slice, simultaneous monitoring of displacement at the focus and temperature distribution during

HIFU ablation in soft tissue, while preserving high duty cycle for efficient acoustic energy deposition. Changes on the order of 20% in tissue displacement was observed during both ex vivo and in vivo MR-HIFU experiments when lethal thermal dose was reached. The use of such a metric may thus be explored in future studies to assess potential tissular modifications during HIFU therapy in complement to conventional thermal dose imaging.

ACKNOWLEDGMENTS

Authors gratefully acknowledge Delphine Vieillot and Virginie Loyer for their assistance in animal experimentation and Pippa McKelvie-Sebileau for manuscript editing.

REFERENCES

1. Ellis S, Rieke V, Kohi M, Westphalen AC. Clinical applications for magnetic resonance guided high intensity focused ultrasound (MRgHIFU): present and future: clinical applications for MRgHIFU. J Med Imaging Radiat Oncol 2013;57:391–399.
2. Jang HJ, Lee J-Y, Lee D-H, Kim W-H, Hwang JH. Current and future clinical applications of High-Intensity Focused Ultrasound (HIFU) for pancreatic cancer. Gut Liver 2010;4(Suppl. 1):S57–S61.
3. Poorter JD. Noninvasive MRI thermometry with the proton resonance frequency method: study of susceptibility effects. Magn Reson Med 1995;34:359–367.
4. Clarke RL, ter Haar GR. Temperature rise recorded during lesion formation by high-intensity focused ultrasound. Ultrasound Med Biol 1997;23:299–306.
5. Brosses ES, Pernot M, Tanter M. The link between tissue elasticity and thermal dose in vivo. Phys Med Biol 2011;56:7755–7765.
6. Ramaekers P, Greef M de, Breugel JMM van, Moonen CTW, Ries M. Increasing the HIFU ablation rate through an MRI-guided sonication strategy using shock waves: feasibility in the in vivo porcine liver. Phys Med Biol 2016;61:1057–1077.
7. Elbes D, Denost Q, Robert B, Köhler MO, Tanter M, Bruno Q. Magnetic resonance imaging for the exploitation of bubble-enhanced heating by high-intensity focused ultrasound: a feasibility study in ex vivo liver. Ultrasound Med Biol 2014;40:956–964.
8. Sokka SD, King R, Hynynen K. MRI-guided gas bubble enhanced ultrasound heating in in vivo rabbit thigh. Phys Med Biol 2003;48:223–241.
9. Zderic V, Foley J, Luo W, Vaezy S. Prevention of post-focal thermal damage by formation of bubbles at the focus during high intensity focused ultrasound therapy. Med Phys 2008;35:4292–4299.
10. McDannold N, Maier SE. Magnetic resonance acoustic radiation force imaging. Med Phys 2008;35:3748–3758.
11. Radicke M, Engelbertz A, Rabenstein B, Lewerenz M, Oehms O, Trautner P, Weber B, Wrede S, Maier K. New image contrast method in magnetic resonance imaging via ultrasound. In Proceedings of the 14th International Conference on Hyperfine Interactions and 18th International Symposium on Nuclear Quadrupole Interactions (HFI/NQI 2007) Iguassu Falls (Puerto Iguazú-Argentina / Foz de Iguaçcu-Brasil), 5–10 August 2007 p 541–546.
12. Kaye EA, Hertzberg Y, Marx M, Werner B, Navon G, Levoy M, Pauly KB. Application of Zernike polynomials towards accelerated adaptive focusing of transcranial high intensity focused ultrasound. Med Phys 2012;39:6254–6263.
13. Hertzberg Y, Volovick A, Zur Y, Medan Y, Vitek S, Navon G. Ultrasound focusing using magnetic resonance acoustic radiation force imaging: application to ultrasound transcranial therapy. Med Phys 2010;37:2934–2942.
14. Tsui P-H, Wang S-H, Huang C-C. In vitro effects of ultrasound with different energies on the conduction properties of neural tissue. Ultrasonics 2005;43:560–565.
15. Mihran RT, Barnes FS, Wachtel H. Temporally-specific modification of myelinated axon excitability in vitro following a single ultrasound pulse. Ultrasound Med Biol 1990;16:297–309.
16. Plaksin M, Shoham S, Kimmel E. Intramembrane cavitation as a predictive bio-piezoelectric mechanism for ultrasonic brain stimulation. Physical review X 2014. http://link.aps.org/doi/10.1103/PhysRevX.4.011004. Accessed May 2, 2016.
17. Mougenot C, Waspe A, Looi T, Drake JM. Variable ultrasound trigger delay for improved magnetic resonance acoustic radiation force imaging. Phys Med Biol 2016;61:712–727.
18. Auboiroux V, Viallon M, Roland J, et al. ARFI-prepared MRgHIFU in liver: simultaneous mapping of ARFI-displacement and temperature elevation, using a fast GRE-EPI sequence. Magn Reson Med 2012;68:932–946.
19. Kaye EA, Pauly KB. Adapting MRI acoustic radiation force imaging for in vivo human brain focused ultrasound applications. Magn Reson Med 2013;69:724–733.
20. Hansen MS, Sørensen TS. Gadgetron: an open source framework for medical image reconstruction. Magn Reson Med 2013;69:1768–1776.
21. de Zwart JA, van Gelderen P, Kelly DJ, Moonen CT. Fast magnetic-resonance temperature imaging. J Magn Reson B 1996;112:86–90.
22. Sapareto SA, Dewey WC. Thermal dose determination in cancer therapy. Int J Radiat Oncol Biol Phys 1984;10:787–800.
23. Dewey WC. Arrhenius relationships from the molecule and cell to the clinic. Int J Hyperthermia 1994;10:457–483.
24. Ozenne V, Toupin S, Bour P, de Senneville BD, et al. Improved cardiac magnetic resonance thermometry and dosimetry for monitoring lesion formation during catheter ablation. Magn Reson Med 2016. doi: 10.1002/mrm.26158.
25. Arnal B, Pernot M, Tanter M. Monitoring of thermal therapy based on shear modulus changes: II. Shear wave imaging of thermal lesions. IEEE Trans Ultrason Ferroelectr Freq Control 2011;58:1603–1611.
26. Maleke C, Konofagou EE. Harmonic motion imaging for focused ultrasound (HMIFU): a fully integrated technique for sonication and monitoring of thermal ablation in tissues. Phys Med Biol 2008;53:1773–1793.
27. Hou GY, Marquet F, Wang S, Apostolakis I-Z, Konofagou EE. High-intensity focused ultrasound monitoring using harmonic motion imaging for focused ultrasound (HMIFU) under boiling or slow denaturation conditions. Ultrason Ferroelectr Freq Control 2015;62:1308–1319.
28. Damianou CA, Sanghvi NT, Fry FJ, Maass-Moreno R. Dependence of ultrasonic attenuation and absorption in dog soft tissues on temperature and thermal dose. J Acoust Soc Am 1997;102:628–634.29.
29. Khokhlova VA, Bailey MR, Reed JA, Cunitz BW, Kaczkowski PJ, Crum LA. Effects of nonlinear propagation, cavitation, and boiling in lesion formation by high intensity focused ultrasound in a gel phantom. J Acoust Soc Am 2006;119:1834–1848.
30. Coluccia D, Fandino J, Schwyzer L, O'Gorman R, Remonda L, Anon J, Martin E, Werner B. First noninvasive thermal ablation of a brain tumor with MR-guided focused ultrasound. J Ther Ultrasound 2014;2:17.
31. Monteith SJ, Medel R, Kassell NF, Wintermark M, Eames M, Snell J, Zadicario E, Grinfeld J, Sheehan JP, Elias WJ. Transcranial magnetic resonance–guided focused ultrasound surgery for trigeminal neuralgia: a cadaveric and laboratory feasibility study: laboratory investigation. J Neurosurg 2013;118:319–328.
32. Chang JW, Min B-K, Kim B-S, Chang WS, Lee Y-H. Neurophysiologic correlates of sonication treatment in patients with essential tremor. Ultrasound Med Biol 2015;41:124–131.
33. Marsac L, Chauvet D, Larrat B, Pernot M, Robert B, Fink M, Boch AL, Aubry JF, Tanter M. MR-guided adaptive focusing of therapeutic ultrasound beams in the human head. Med Phys 2012;39:1141–1149.
34. Mast TD, Salgaonkar VA, Karunakaran C, Besse JA, Datta S, Holland CK. Acoustic emissions during 3.1 MHz ultrasound bulk ablation in vitro. Ultrasound Med Biol 2008;34:1434–1448.
35. de Senneville BD, Mougenot C, Moonen CTW. Real-time adaptive methods for treatment of mobile organs by MRI-controlled high-intensity focused ultrasound. Magn Reson Med 2007;57:319–330.